Nanoscale Advances

ROYAL SOCIETY OF CHEMISTRY

PAPER

View Article Online
View Journal | View Issue

Cite this: *Nanoscale Adv.*, 2026, **8**, 2604

High thermal nonlinearity in thin films of Zn-doped CuS QDs dispersed in a PMMA matrix for NLO applications

G. G. Muley,[a] Y. S. Tamgadge, *[b] P. P. Gedam[c] and R. P. Ganorkar[d]

We report improved thermally stimulated third-order nonlinear optical coefficients (nonlinear refraction and nonlinear absorption) in thin films of Zn-doped CuS quantum dots (QDs) dispersed in a poly (methyl methacrylate) (PMMA) matrix. Undoped and Zn-doped (1, 2, and 3 wt%) CuS QDs were synthesized using a co-precipitation method. Powder samples were characterized using X-ray diffraction (XRD), high-resolution transmission electron microscopy (HR-TEM), ultraviolet-visible (UV-vis) spectroscopy, and open- and closed-aperture *z*-scan technique. The XRD spectra confirmed the formation of a highly pure covellite CuS phase with a hexagonal crystal structure in the $P6_3/mmc$ (194) space group. The EDS analysis validated the purity of the synthesized samples. HR-TEM micrographs of 1 wt% Zn-doped CuS QDs clearly showed the formation of very narrow-sized Zn-doped CuS QDs with average sizes of 2–3 nm. A strong blue-shift in the maximum absorption wavelength is observed for the 3 wt% Zn-doped sample with a band gap of 2.24 eV. Considerably enhanced third-order nonlinear refraction and absorption coefficients were obtained for the 3 wt% Zn-CuS-PMMA nanocomposite thin films, indicating their potential use in optical limiters and photonic devices.

Received 19th July 2025
Accepted 6th March 2026

DOI: 10.1039/d5na00695c

rsc.li/nanoscale-advances

1. Introduction

Nanostructured metal sulfides (ZnS, CdS, and CuS) have attracted tremendous attention because their optical, physical, chemical and electronic properties can be modified and tuned to desired levels.[1–4] Their natural abundance, non-toxicity, low cost and excellent properties at the nanoscale make them prominent candidates for potential applications in solar cell devices, supercapacitors, optoelectronic devices, photocatalysts, and energy storage.[1,3,5–7] Copper sulfide (CuS), a p-type semiconducting nanostructure, is the most popular among other metal sulfides due to its distinct absorption properties in the near-infrared region, showing extensive applications in solar cells, lithium-ion batteries, energy conversion materials, photocatalytic materials, nonlinear optical (NLO) materials, and sensors.[4,8–16] Various studies have highlighted the significant role of dopants and surface passivating agents in tuning and optimizing the electrical, optical, mechanical, and structural properties of CuS nanoparticles (NPs).[13,17–24] The nonlinear interaction of laser beam with materials results in many NLO effects including self-focusing, self-defocusing, nonlinear refraction, nonlinear absorption, excited-state absorption, self-phase modulation, and second- and multi-order harmonic generation.[25–27] Materials capable of showing such properties are potentially used in various NLO devices such as all-optical switching devices, optical limiters, second- and multi-order harmonic generators, and lasers.[25,27,28] Semiconducting NPs and polymer-NP composites are known to exhibit excellent NLO properties.[29–32] Poly(methyl methacrylate) (PMMA) has been studied widely due to its high NLO coefficients.[33–36] However, very few studies have been performed to investigate the NLO properties of CuS quantum dots (QDs) and their composites with PMMA.

The present study highlights a strong third-order response dominated by thermal nonlinearity, and it is important to recognize the implications of this mechanism for practical photonic applications. Thermal nonlinearities arise from laser-induced heating, which leads to refractive index changes *via* thermo-optic coefficients and local thermal diffusion.[37] These nonlinearities typically occur on microsecond-millisecond timescales, making them many orders of magnitude slower than the purely electronic nonlinearities that respond on the femtosecond-picosecond timescale.[38] As a consequence, thermally driven nonlinearities are well suited for applications such as optical limiting, optical switching at low frequencies, beam shaping, and intensity-dependent attenuation, in which a slower but strong nonlinear response is advantageous.[39]

[a]*Department of Physics, Sant Gadge Baba Amravati University, Amravati (MS) 444602, India*

[b]*Department of Physics, Mahatma Fule Arts, Commerce & Sitaramji Chaudhari Science Mahavidyalaya, Warud, Amravati (MS) 444906, India. E-mail: ystamgadge@gmail.com*

[c]*Department of Physics, Shri R.L. T. College of Science, Akola (MS)444001, India*

[d]*Department of Chemistry, Mahatma Fule Arts, Commerce & Sitaramji Chaudhari Science Mahavidyalaya, Warud, Amravati (MS) 444906, India*

However, the relatively slow recovery time limits their application in ultrafast photonic circuits, all-optical logic gates, and high-speed telecommunications, where rapid modulation requires fast electronic (Kerr-type) nonlinearities.[40]

In Zn-doped CuS-PMMA films, the enhanced nonlinearity likely originates from heat accumulation around the nanoparticles due to the strong absorption and localized defect states introduced by Zn substitution, which increase non-radiative relaxation pathways. While this thermal contribution significantly boosts the magnitude of n_2 and the optical limiting threshold, it implies that device performance will depend strongly on thermal management, diffusion rates within the polymer matrix, and pulse duration of the incident light. These characteristics should therefore be considered when assessing the suitability of such materials for incorporation in high-speed photonic systems.[41,42] Overall, the observed thermal nonlinearity is beneficial for optical limiting and protective photonics, but it imposes fundamental constraints for ultrafast all-optical switching. In this work, we report the synthesis of Zn-doped CuS QDs by a simple co-precipitation method and investigate the NLO properties of thin films obtained from QDs-PMMA nanocomposites. L-alanine (an amino acid) is utilized as a capping agent, and Zn-doped CuS QDs are characterized for gaining insights into their various structural and optical properties.

2. Experimental

2.1 Materials

Zinc chloride (dry) ($ZnCl_2$), sodium sulfide flakes 50% (Na_2S), copper chloride dihydrate ($CuCl_2 \cdot 2H_2O$), acetone, and ethanol were purchased from SD-Fine Chem Ltd, India. PMMA and L-alanine were procured from Sigma-Aldrich, USA. Double-distilled water (DDW) was used as the solvent for the synthesis of QDs, and acetone was used as the solvent for preparing the QDs-PMMA thin films.

2.2 Synthesis of L-alanine-capped Zn-doped CuS QDs and preparation of the thin films

Undoped and Zn-doped CuS QDs capped with L-alanine were synthesized by a simple co-precipitation method. In a typical synthesis process of 1 wt% Zn-doped CuS QDs (sample name CZ1), 10 mL of 1 M copper chloride dihydrate solution was taken in a fresh beaker containing 50 mL of DDW and vigorously stirred using a magnetic stirrer for 30 min. The temperature of the solution was maintained at 80 °C. The stoichiometric amount of zinc chloride powder corresponding to 1 wt% doping in CuS was added to the copper chloride solution and stirred for additional 30 min. 10 mL of L-alanine (0.1 M) was then added under stirring for another 30 min. The temperature of the solution was then brought down to 30 °C, and 10 mL of 2 M sodium sulfide solution was added dropwise, resulting in the formation of a black-coloured precipitate (ppt) of 1 wt% Zn-doped CuS QDs. The precipitate was filtered by Whatman's filter paper and dried in a hot air oven at 80 °C for 2 h. Two more samples of Zn-doped CuS QDs were prepared by repeating the above procedure with sample names CZ2 and CZ3 for the 2 wt% and 3 wt% Zn-doping, respectively. Sample CS was prepared without the use of Zn. Dried precipitates of all samples were crushed using an agate mortar and pestle, and the fine black powders of the QDs were used for further characterization.

Thin films of these QDs-PMMA were prepared by a spin coating technique. For this purpose, an estimated amount of CZ1 QDs powder was taken in a fresh beaker containing 10 mL of acetone, yielding 1 mM CZ1 dispersion. A stable dispersion was obtained by keeping the beaker in an ultrasonic bath for 30 min. In another beaker, 10 ml of 0.1% PMMA solution in acetone was prepared. The two solutions were combined under constant stirring and further treated in an ultrasonic bath for 30 min to achieve uniform dispersion of QDs within the PMMA matrix. The resultant suspension was subsequently utilized for thin-film fabrication of the sample, denoted as CZ1-PMMA, using the spin-coating technique. Similarly, thin-film samples CZ2-PMMA, CZ3-PMMA and CS-PMMA were also prepared.

2.3 Characterization

All synthesized QDs were characterized for investigating their structural, morphological, linear and nonlinear optical properties. Crystal structures were investigated by X-ray diffraction (XRD) technique using an X-ray powder diffractometer, Rigaku MiniFlex 600. Elemental purity analysis was carried out *via* energy-dispersive X-ray spectroscopy (EDS) using a field emission gun-scanning electron microscope (FEG-SEM), Model JSM-

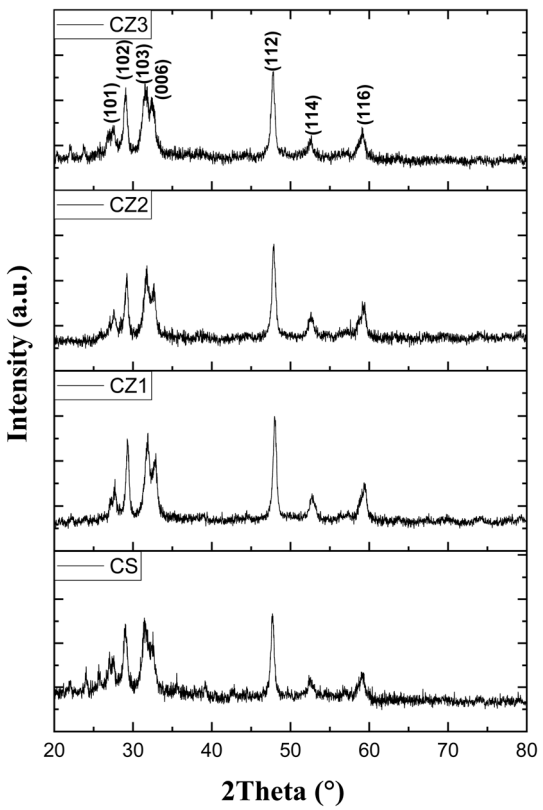

Fig. 1 XRD spectra of undoped and Zn-doped CuS NPs.

7600F, Japan, operated at an accelerating voltage of 200 kV. High-resolution transmission electron microscopy (HR-TEM) was performed for morphological studies using FEG-TEM 300 KV Model FEI Tecnai G2, F30 operated at an accelerating voltage of 300 kV. Linear optical studies were performed by ultraviolet-visible (UV-vis) absorption spectroscopy using a UV-visible spectrophotometer (BLK-C-SR, Stellarnet, USA) in the wavelength range of 190–1100 nm.

3. Results and discussion

3.1 XRD, EDS and HR-TEM studies

The powder samples of QDs were subjected to XRD study for the evaluation of crystal structure and lattice parameters. CuKα radiations with a wavelength of 1.54059 Å were used at an operating voltage of 40 kV and 15 mA current. The powder samples were scanned at 2θ values between 20–80°, and all significant intensity peaks were recorded. Fig. 1 illustrates the XRD spectra recorded for all undoped and Zn-doped CuS QDs. XRD peaks in the spectrum are broadened, which is a clear indication of the existence of samples with a narrow crystallite size. The crystallite size of all samples was calculated using the Debye–Scherrer formula and is shown in Table 2. These data also confirm the formation of CuS QDs with particle sizes of 5–7 nm, and the particle size is found to decrease with increasing Zn-doping concentration: the 3 wt% Zn-doped CuS QDs exhibited the least particle size (5 nm). All diffraction peaks matched well with the standard data and are indexed as per PDF Card Nos.: 9000523, 9008389 and 9000062. XRD spectra confirmed the formation of a covellite CuS phase with a hexagonal crystal structure in the $P6_3/mmc$ (194) space group. The corresponding cell parameters are presented in Table 1. The absence of impurity peaks corresponding to any undesired phases validates the purity of the synthesized samples.

The purity of the prepared samples were investigated by EDS spectrum. Fig. 2 depicts the EDS spectrum of 1 wt% Zn-doped CuS QDs. Only the peaks and energy values associated with the Cu, S and Zn elements were observed, and no impurity elements were detected. This observation validates the purity of the synthesized samples. Fig. 3 illustrates the HR-TEM micrographs of 1 wt% Zn-doped CuS QDs. They clearly show the formation of very narrow-sized Zn-doped CuS QDs that are distinctly separated from each other. QDs are uniformly distributed and are of nearly spherical in shape with dimensions in the range of 2–3 nm. The crystallite size estimated from XRD using the Debye–Scherrer equation should be considered an approximate value as it is sensitive to instrumental broadening, lattice strain, and peak selection. The smaller particle size observed in the HR-TEM analysis may arise from the projection effects, limited sampling, and partial visibility of crystallites. Such discrepancies between XRD- and TEM-derived sizes have been widely reported for ultrasmall nanomaterials.

3.2 Linear optical studies using UV-vis spectra

Linear optical properties of all synthesized QDs were studied using UV-vis absorption spectroscopy, and optical band gaps for

Table 1 XRD parameters of CuS NPs

	Cell parameters						
Sample name	*a*	*b*	*c*	Alpha	Beta	Gamma	Volume
CS	3.7938	3.7938	16.3410	90.000	90.000	120.000	203.685
CZ1	3.7938	3.7938	16.3410	90.000	90.000	120.000	203.685
CZ2	3.7960	3.7960	16.3600	90.000	90.000	120.000	204.158
CZ3	3.7820	3.7820	16.2900	90.000	90.000	120.000	201.788

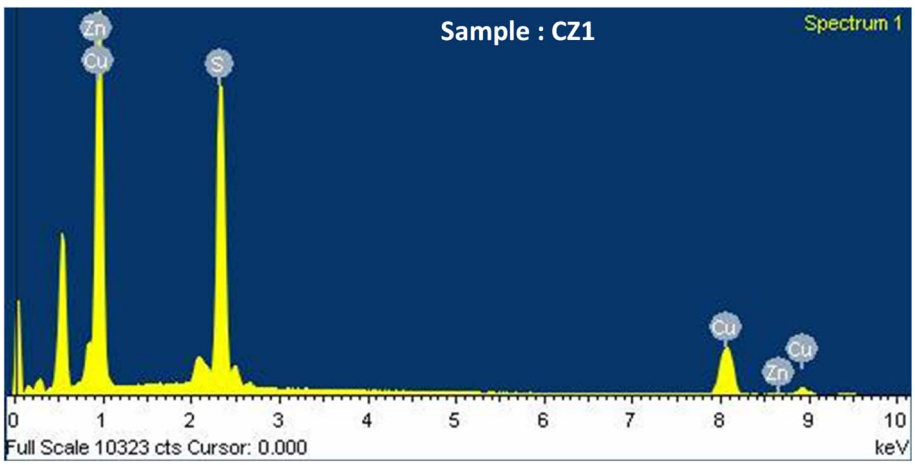

Fig. 2 EDS spectrum of Zn-doped CuS NPs.

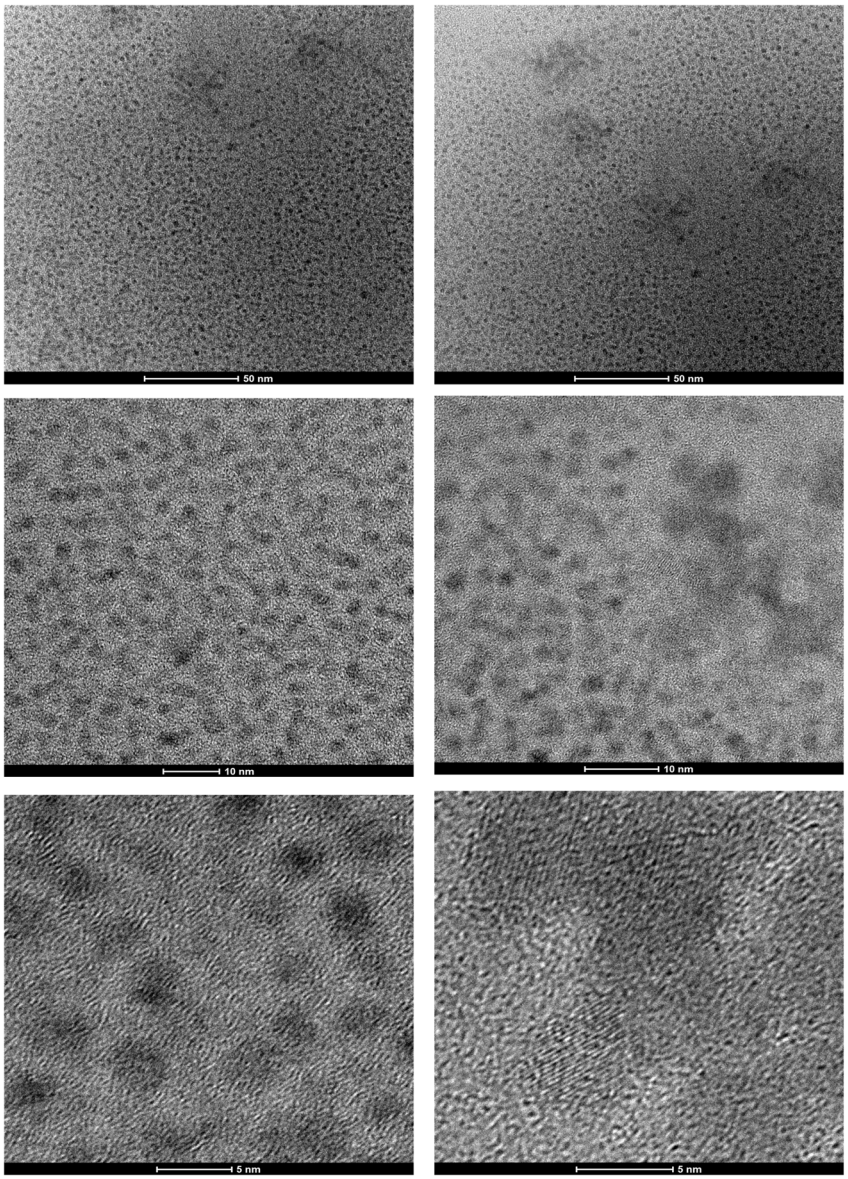

Fig. 3 HR-TEM micrographs of Zn-doped CuS NPs.

all the samples were calculated using the procedure described by Tauc. Fig. 4(a) depicts the portion of the absorption spectra of all samples in the wavelength range of 570–730 nm. The spectra depicted broad absorption peaks from 630–640 nm with a wavelength width of approximately 10 nm. A blue shift in the maximum absorption wavelength was observed upon the doping of Zn into the CuS lattice. The maximum shift was recorded for the 3 wt% Zn-doped sample. This suggested that Zn might have occupied the vacancy sites in the CuS lattice, which was not favourable for the growth in crystallite size. The blue-shift in the absorption peaks was the result of the increased band gap energy. This fact was verified by drawing the Tauc plots for all samples and estimating the band gap energy for each sample by extending the linear portion of the curve on the photon energy axis. The point at which this extrapolation intersects the photon energy axis corresponds to the energy band gap. Fig. 4(b) shows the Tauc plots obtained for all the samples. Estimated band gap energies were found to increase with increasing Zn-doping concentration. The 3 wt% Zn-doped CuS QDs were found to exhibit the largest band gap of 2.24 eV. The optical parameters of all samples are tabulated in Table 2.

3.3 Nonlinear refraction studies of undoped and Zn-doped CuS-PMMA thin films

Third-order nonlinear refraction was investigated in undoped and Zn-doped CuS QDs dispersed in a PMMA host matrix in the form of thin films using a closed-aperture configuration of the single-beam z scan technique, as described by M. Sheik and

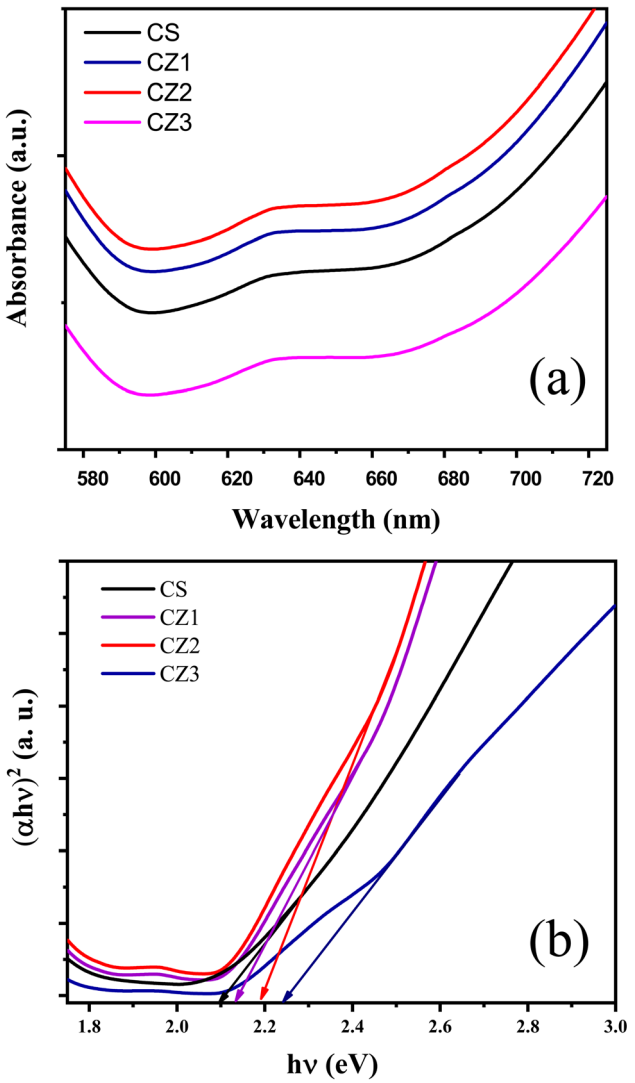

Fig. 4 (a) Absorption spectra and (b) Tauc plots for undoped and Zn-doped CuS NPs.

Table 2 Optical and structural parameters of CuS NPs

Sample name	Absorption peak (nm)	Optical band gap (eV)	Average crystallite size (nm)	
			XRD	TEM
CS	638	2.08	7	—
CZ1	635	2.13	7	3
CZ2	633	2.19	6	—
CZ3	630	2.24	5	—

Bahae *et al.*.[43,44] A linearly polarized helium-neon laser (10 mW) with a Gaussian beam profile was focused using a 20 cm convex lens on the thin-film sample. The sample was then scanned at different pre-focal to post-focal positions along beam direction, and the output transmittance was recorded using the aperture before the detector. The laser beam upon interacting with the sample produces a nonlinear response (third-order) at the same frequency of the incident beam.[29] The presence of the aperture produces an output transmittance that is sensitive to phase distortion, and the intensity-dependent nonlinear refractive index n_2 can be evaluated using the following equations:[25,27,28]

$$n_2 = \frac{3}{2n_0^2\varepsilon_0 c}\chi^{(3)}, \quad (1)$$

$$n_2 = \frac{\Delta T_{pv}}{kI_0 L_{eff} 0.406(1-S)^{0.27}}, \quad (2)$$

where ΔT_{pv} is the change in the peak-to-valley transmittance, S is the aperture transmittance (0.3 in the present case), while the other symbols have their usual meanings. Fig. 5 depicts the closed-aperture z-scan curves for the prepared thin-film samples. All the curves exhibited a pre-focal maximum followed by a post-focal minimum, which indicated that the nanocomposites showed negative lensing due to the self-defocusing effect.[26,27] Experimental curves were fitted with theoretical equations, which showed good agreement with the observed behaviour. A very large value of nonlinear refractive index n_2 was obtained for all samples. Its value was found to increase with Zn-dopant concentration, and CZ3-PMMA attained the maximum value, as shown in Table 3. This considerable enhancement may be attributed to the non-local heating of the samples. This nonlinearity, attributed to thermal effects, is further confirmed by the separation between the peak and valley, which is greater than $1.7z_0$. The continuous exposure of the samples to a cw laser creates a rise in temperature that generates phonons, which propagate within these samples. The interaction of the incident laser beam with phonons develops a piezo-optical or photo-elastic effect, generating an enhanced third-order effect. The enhancement might also be due to the anharmonic behaviour of the CuS lattice caused by doping.[13,15,21,45–49]

Zn-doping markedly enhance the third-order NLO response of metal chalcogenide-polymer nanocomposites by altering their electronic configuration, defect landscape, and interfacial dielectric environment.[50–52] In CuS systems, the partial substitution of Cu^{+}/Cu^{2+} ions with Zn^{2+} induces lattice distortions and introduces additional localized states within the band structure, thereby increasing the density of intermediate levels available for nonlinear electronic transitions.[50,53] Such modifications frequently coincide with reduced crystallite sizes and stronger quantum confinement, which increase the oscillator strength of excitonic and intraband transitions and consequently amplify the $\chi^{(3)}$ response.[51,53] Moreover, Zn-incorporation can tune the intrinsic local surface plasmon resonance of the p-type CuS, leading to enhanced local electromagnetic fields and strengthened nonlinear refractive and reverse saturable absorption processes through plasmon-assisted carrier excitation. When embedded in a PMMA matrix, Zn-doped CuS nanoparticles further benefit from improved dispersion and interfacial polarization, enabling

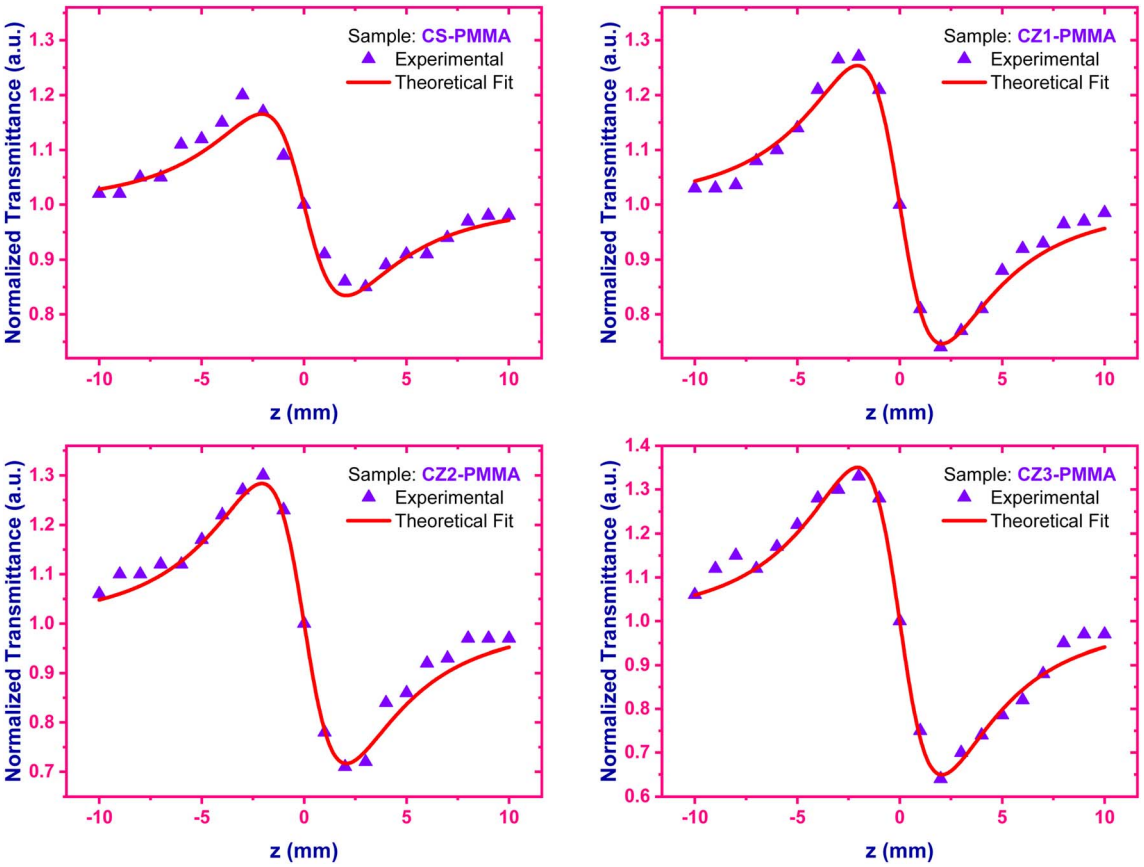

Fig. 5 Closed-aperture *z*-scan curves for undoped and Zn-doped CuS-PMMA thin films.

Table 3 NLO coefficients of the as-prepared nanocomposite thin films

		NLO coefficients				
Sample name	Thickness (nm)	$n_2 \times 10^{-4}$ (cm^2 w^{-1})	$\beta \times 10^{-4}$ (cm^2 w^{-1})	Re[$\chi^{(3)}$] $\times 10^{-2}$ esu	Im[$\chi^{(3)}$] $\times 10^{-9}$ esu	$\chi_{eff}^{(3)} \times 10^{-2}$ esu
CS-PMMA	213	3.15	2.20	3.26	1.13	3.26
CZ1-PMMA	264	4.05	3.87	4.22	2.00	4.22
CZ2-PMMA	212	5.82	4.82	6.04	2.48	6.04
CZ3-PMMA	231	6.43	7.60	6.67	3.92	6.67

more efficient optical field coupling and spatially uniform nonlinear interaction throughout the films. These synergistic structural and electronic effects collectively account for the substantial enhancement in third-order NLO coefficients observed in Zn-modified CuS-PMMA nanocomposite thin films.[50]

3.4 Nonlinear absorption studies of undoped and Zn-doped CuS-PMMA thin films

An open-aperture *z*-scan configuration was utilized to determine the third-order nonlinear absorption processes taking place in the samples, thereby evaluating the nonlinear absorption coefficient β. In this configuration, the output transmittance is recorded without the use of an aperture in the far-field, making the transmitted power independent of nonlinear refractions and solely dependent on the absorption process. Fig. 6 shows the open-aperture *z*-scan curves exhibiting a valley at the focal position, indicating the occurrence of a reverse saturable absorption process. All samples showed improvement in the coefficient β, which was obtained from the nonlinear theoretical fit, closely resembling the experimental data. The nonlinear absorption coefficient β attained the maximum value for the sample doped with 3 wt% Zn into CuS QDs. This considerable enhancement may be attributed to the dielectric effect, surface state effects, and quantum confinement effect.[12,47,54] Table 4 shows the NLO coefficients of some previously reported nonlinear materials. Significant improvement in NLO properties observed in the present work suggest their

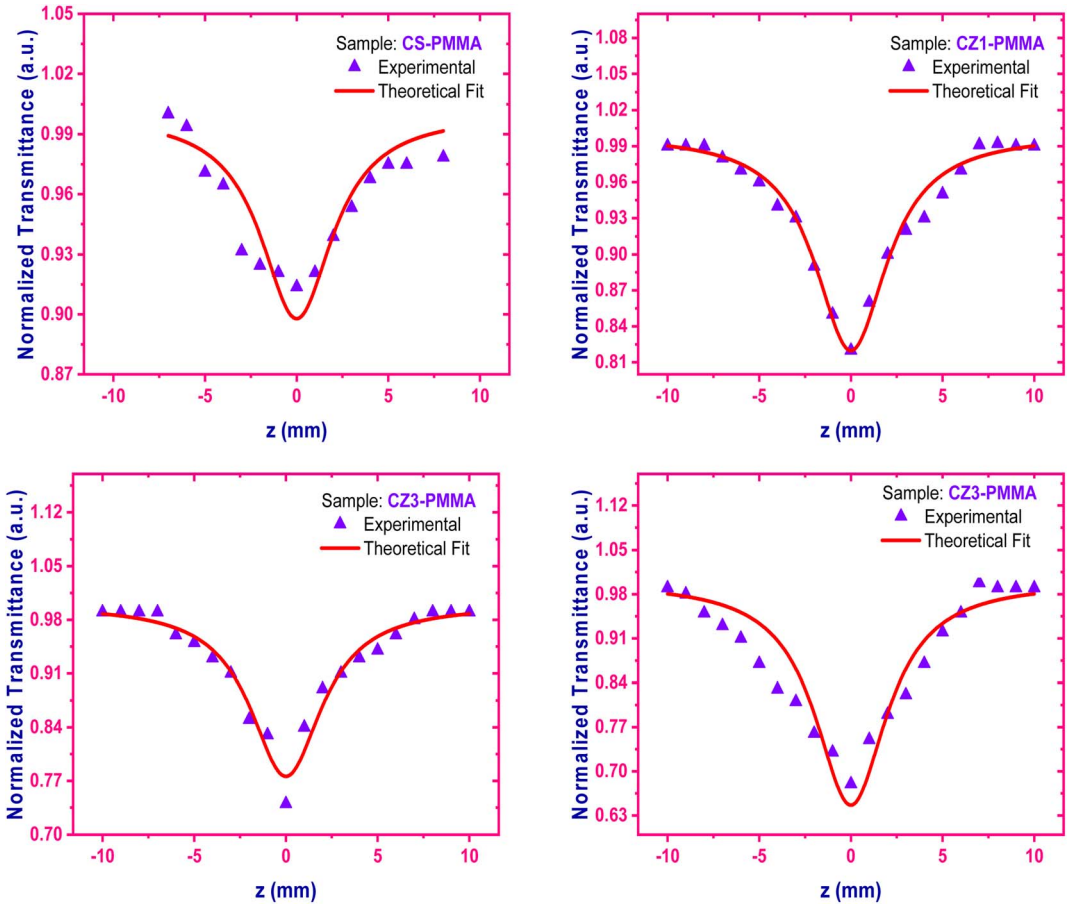

Fig. 6 Open-aperture *z*-scan curves for undoped and Zn-doped CuS-PMMA thin films.

Table 4 NLO coefficients (thermal origin) reported in previous studies

Sr. No.	Nonlinear material	n_2	β	χ_{eff}
1	Sr-doped ZnO-PVA thin-film[24]	5.79×10^{-4} cm^2 W^{-1}	6.57×10^{-4} cm W^{-1}	0.591×10^{-3} esu
2	Cd-doped CuO-PVA thin-film[55]	38.9×10^{-5} cm^2 W^{-1}	11.0×10^{-6} cm W^{-1}	68.2×10^{-3} esu
3	(PVA) with 1 wt% of Fe_2O_3 or NiO nanoparticles[56]	53.5×10^{-13} esu	—	26.6×10^{-14} esu
4	ZnO-doped polyvinyl alcohol/polyvinyl pyrrolidone (PVA/PVP) polymeric films[57]	11.37×10^{-11} esu	—	78.913×10^{-13} esu
5	Zinc-oxide-encapsulated poly (vinyl alcohol) nanocomposite films[58]	—	0.208×10^{-3} cm W^{-1}	—
6	TiO_2-polystyrene nanocomposite films[59]	14.43×10^{-12} m^2 W^{-1}	3.76×10^{-5} m W^{-1}	—
7	MoS_2/PVA nanocomposites[60]	4.21×10^{-5} cm^2 W^{-1}	4.24×10^{-6} cm W^{-1}	1.68×10^{-3} esu
8	P (st-*co*-MMA)/NiO polymer nanocomposites[61]	5.93×10^{-8} cm^2 W^{-1}	6.72×10^{-4} cm W^{-1}	33.85×10^{-7} esu
9	$MoSe_2$/PVA nanocomposites[62]	5.25×10^{-6} cm^2 W^{-1}	8.97×10^{-7} cm W^{-1}	6.2×10^{-7} esu
10	Sr-doped CuO-PVA thin-film[45]	31.3×10^{-5} cm^2 W^{-1}	4.54×10^{-6} cm W^{-1}	54.7×10^{-3} esu
11	Cu-doped ZnO-PVA thin-film[63]	6.35×10^{-4} cm^2 W^{-1}	7×10^{-4} cm W^{-1}	0.649×10^{-3} esu

potential applications in optoelectronics devices, photonics, all-optical switching devices, *etc.*[13,17,47]

4. Conclusions

Thermally stimulated third-order nonlinear optical coefficients of Zn-doped CuS QDs dispersed into a PMMA matrix in the form of nanocomposite thin films were investigated using the *z*-scan technique. Undoped and 1, 2, and 3 wt% Zn-doped CuS QDs were successfully synthesized using the co-precipitation method. Powder samples were characterized by XRD, HR-TEM, UV-vis spectroscopy, and open- and closed-aperture *z*-scan technique. The XRD spectra confirmed the formation of the highly pure covellite CuS phase with a hexagonal crystal structure. EDS and HR-TEM analyses validated Zn-doping into

CuS QDs and confirmed the formation of uniformly dispersed near-zero-dimensional Zn-doped CuS QDs with average particle sizes of 2–3 nm. A strong blue shift in the absorption wavelength and an increased optical band gap of 2.24 eV were observed for the 3 wt% Zn-doped sample. Significantly improved n_2 and β values were obtained for the 3 wt% Zn-CuS-PMMA nanocomposite thin films, making them potentially useful for optical limiters and photonic devices.

Conflicts of interest

There are no conflicts to declare.

Data availability

The data supporting this article will be made available as and when requested.

Supplementary information (SI): raw XRD data files. See DOI: https://doi.org/10.1039/d5na00695c.

Acknowledgements

The authors acknowledge DST and SAIF/CRNTS, IIT Bombay, for providing the field emission gun-scanning electron microscope (FEG-SEM) and field emission gun transmission electron microscope (FEG-TEM) facilities for our research work.

References

1 C.-H. Lai, M.-Y. Lu and L.-J. Chen, *J. Mater. Chem.*, 2012, **22**, 19–30.
2 S. Riyaz, A. Parveen and A. Azam, *Perspect. Sci.*, 2016, **8**, 632–635.
3 A. P. Alivisatos, *Science*, 1996, **271**, 933–937.
4 M. Khademian, M. Zandi, M. Amirhoseiny and D. Dorranian, *J. Cluster Sci.*, 2017, **28**, 2753–2764.
5 M. J. Paul, R. Suresh, K. T. Valavan, R. Marnadu, M. Vidhya, N. Ahmad, A. M. Alshehri and S. Gedi, *J. Alloys Compd.*, 2021, **886**, 161196.
6 F. Khan, I. Fareed, M. Al-Rasheidi, N. Ahmad, A. Al-Ahmed, Z. M. Ahmed, M. Shariq and Md. H. Zahir, *Inorg. Chem. Commun.*, 2022, **135**, 109094.
7 A. Nekooei, M. R. Miroliaei, M. Shahabi Nejad and H. Sheibani, *Mater. Sci. Eng. B*, 2022, **284**, 115884.
8 H. Lee, S. W. Yoon, E. J. Kim and J. Park, *Nano Lett.*, 2007, **7**, 778–784.
9 A. E. Raevskaya, A. L. Stroyuk, S. Ya. Kuchmii and A. I. Kryukov, *J. Mol. Catal. A: Chem.*, 2004, **212**, 259–265.
10 Y. Wang, X. Zhang, P. Chen, H. Liao and S. Cheng, *Electrochim. Acta*, 2012, **80**, 264–268.
11 R. S. Mane and C. D. Lokhande, *Mater. Chem. Phys.*, 2000, **65**, 1–31.
12 A. M. Malyarevich, K. V. Yumashev, N. N. Posnov, V. P. Mikhailov, V. S. Gurin, V. B. Prokopenko, A. A. Alexeenko and I. M. Melnichenko, *J. Appl. Phys.*, 2000, **87**, 212–216.
13 N. Ahmad, A. M. Alshehri, Z. R. Khan, S. A. M. Almahdawi, M. Shkir, P. M. Z. Hasan, A. Alshahrie, F. Khan and A. Al-Ahmed, *Inorg. Chem. Commun.*, 2022, **139**, 109363.
14 Z. Q. Mamiyev and N. O. Balayeva, *Mendeleev Commun.*, 2016, **26**, 235–237.
15 K. A. Ann Mary, N. V. Unnikrishnan and R. Philip, *Phys. E Low-dimens. Syst. Nanostruct.*, 2015, **74**, 151–155.
16 K. V. G. Raghavendra, K. Alamara, M. Y. Al-Haik, C. V. V. Muralee Gopi, S. Alzahmi, Y. Haik, T. U. K. Nutakki, I. M. Obaidat and K. Madhusudana Rao, *J. Energy Storage*, 2024, **103**, 114312.
17 C. Selvakumar, V. T. Geetha, S. Sathiyamoorthi, R. Sharan and J. Nonlinear Optic, *Phys. Met.*, 2025, **34**, 2450037.
18 R. Zeinodin, F. Jamali-Sheini and M. Cheraghizade, *Mater. Sci. Semicond. Process.*, 2021, **123**, 105501.
19 N. Ahmad, A. M. Alshehri, I. Ahmad, M. Shkir, P. M. Z. Hasan and A. A. Melaibari, *Surf. Interfaces*, 2021, **27**, 101536.
20 N. Ahmad, S. A. M. Almahdawi, A. M. Alshehri, M. Shkir, I. Ahmad, P. M. Z. Hasan and A. A. Melaibari, *Mater. Chem. Phys.*, 2022, **277**, 125552.
21 M. Karthika, A. R. Balu, G. Vinitha, Z. Delci, M. Suganya, S. Chitra Devi, K. Devendran and M. Sriramraj, *Ceram. Int.*, 2023, **49**, 17806–17817.
22 K. Subramanyam, N. Sreelekha, D. Amaranatha Reddy, G. Murali, K. Rahul Varma and R. P. Vijayalakshmi, *Solid State Sci.*, 2017, **65**, 68–78.
23 S. S. Talwatkar, Y. S. Tamgadge, A. L. Sunatkari, A. B. Gambhire and G. G. Muley, *Solid State Sci.*, 2014, **38**, 42–48.
24 Y. S. Tamgadge, A. L. Sunatkari, S. S. Talwatkar, V. G. Pahurkar and G. G. Muley, *Opt. Mater.*, 2014, **37**, 42–50.
25 R. W. Boyd, S. G. Lukishova and Y. R. Shen, ed., in. *Self-focusing: Past and Present: Fundamentals and Prospects*, Springer New York, New York, NY, 2009, vol. 114.
26 G. New, *Introduction to Nonlinear Optics*, Cambridge University Press, Cambridge, 2011.
27 R. W. Boyd, *Nonlinear Optics*, Academic Press, 4th edn, 2020.
28 N. Bloembergen, *Nonlinear Optics: a Lecture Note and Reprint Volume*, New York, W.A. Benjamin, 1965.
29 Y. S. Tamgadge, P. P. Gedam, G. S. Mendhe, R. P. Ganorkar, G. G. Muley and J. Nonlinear Optic, *Phys. Met.*, 2024, 2430002.
30 R. A. Roy and R. Roy, *Mater. Res. Bull.*, 1984, **19**, 169–177.
31 R. Roy, *MRS Online Proc. Libr.*, 1992, **286**, 241–250.
32 B. Lee and S. Komarneni, ed., in. *Chemical Processing of Ceramics*, CRC Press, Boca Raton, 2nd edn, 2005.
33 F. D'Amore, M. Lanata, S. M. Pietralunga, M. C. Gallazzi and G. Zerbi, *Opt. Mater.*, 2004, **24**, 661–665.
34 B. Chen, D. Fang, L. Chen, X. Shen, J. Wei, D. Wang, Q. Zhang, Q. Ouyang, X. Fang and X. Chen, *Mater. Chem. Phys.*, 2023, **309**, 128310.
35 A. H. Yuwono, B. Liu, J. Xue, J. Wang, H. I. Elim, W. Ji, Y. Li and T. J. White, *J. Mater. Chem.*, 2004, **14**, 2978–2987.
36 Z. Qin, C. Fang, Q. Pan, Q. Gu, F. Chen, F. Li and J. Yu, *J. Mater. Sci.*, 2002, **37**, 4849–4852.
37 I. W. Un and Y. Sivan, *Phys. Rev. Mater.*, 2020, **4**, 105201.
38 Y. Sivan and S.-W. Chu, *Nanophotonics*, 2017, **6**, 317–328.

39 Y. Zhang and Y. Wang, *RSC Adv.*, 2017, **7**, 45129–45144.
40 J. Hu, J. Wu, D. Jin, S. T. Chu, B. E. Little, D. Huang, R. Morandotti and D. J. Moss, *Sensors*, 2023, **23**, 9767.
41 N. G. Semaltianos, *Nanomaterials*, 2025, **15**, 55.
42 G. F. Sinclair, N. A. Tyler, D. Sahin, J. Barreto and M. G. Thompson, *Phys. Rev. Appl.*, 2019, **11**, 044084.
43 M. Sheik-Bahae, A. A. Said, T.-H. Wei, D. J. Hagan and E. W. Van Stryland, *IEEE J. Quantum Electron.*, 1990, **26**, 760–769.
44 M. Sheik-bahae, A. A. Said and E. W. Van Stryland, *Opt. Lett.*, 1989, **14**, 955.
45 Y. S. Tamgadge, S. S. Talwatkar, A. L. Sunatkari, V. G. Pahurkar and G. G. Muley, *Thin Solid Films*, 2015, **595**, 48–55.
46 J. Ebothe, W. Gruhn, A. Elhichou, I. V. Kityk, R. Dounia and M. Addou, *Opt Laser. Technol.*, 2004, **36**, 173–180.
47 H. N. Abd, H. L. Saadon and S. J. Abbas, *Opt. Mater.*, 2024, **148**, 114837.
48 N. V. Kamanina, J. Owsik and B. Rusek, *Opt. Appl.*, 2013, 1429–7507, DOI: 10.5277/OA130306.
49 J. Ebothé, R. Miedzinski, V. Kapustianyk, B. Turko, B. Kulyk, W. Gruhn and I. V. Kityk, *J. Phys.: Conf. Ser.*, 2007, **79**, 012001.
50 A. Shukla, S. Shao, S. Carter-Searjeant, S. Haigh, D. Richards, M. Green and A. V. Zayats, *Nanoscale*, 2023, **15**, 3730–3736.
51 S. Yuvaraj, N. Manikandan and G. Vinitha, *Photon. Nanostruct: Fundam. Appl.*, 2021, **45**, 100922.
52 Y. Hamanaka, T. Hirose, K. Yamada and T. Kuzuya, *Opt. Mater. Express*, 2016, **6**, 3838–3848.
53 R. Bairy, P. shankaragouda Patil, S. R. Maidur, V. H, M. M. S and U. B. K, *RSC Adv.*, 2019, **9**, 22302–22312.
54 S. Gross, D. Camozzo, V. Di Noto, L. Armelao and E. Tondello, *Eur. Polym. J.*, 2007, **43**, 673–696.
55 Y. S. Tamgadge, V. G. Pahurkar, S. S. Talwatkar, A. L. Sunatkari and G. G. Muley, *Appl. Phys. B*, 2015, **120**, 373–381.
56 M. Rashad, *Opt. Mater.*, 2020, **105**, 109857.
57 S. H. Zyoud, T. H. AlAbdulaal, A. Almoadi, M. S. Alqahtani, F. A. Harraz, M. S. Al-Assiri, I. S. Yahia, H. Y. Zahran, M. I. Mohammed and M. S. Abdel-wahab, *Crystals*, 2023, **13**, 608.
58 V. Viswanath, S. S. Nair, G. Subodh and C. I. Muneera, *Mater. Res. Bull.*, 2019, **112**, 281–291.
59 M. Zeinali, B. Jaleh, M. R. R. Vaziri and A. Omidvar, *Quantum Electron.*, 2019, **49**, 951.
60 K. Anand, R. Kaur, A. Arora and S. K. Tripathi, *Opt. Mater.*, 2023, **137**, 113523.
61 M. P. Boranna, P. S. Patil, N. B. Gummagol and H. B. Ravikumar, *Opt. Mater.*, 2023, **140**, 113843.
62 R. Kaur, K. P. Singh and S. K. Tripathi, *J. Alloys Compd.*, 2022, **905**, 164103.
63 Y. S. Tamgadge, A. L. Sunatkari, S. S. Talwatkar, V. G. Pahurkar and G. G. Muley, *Opt. Mater.*, 2016, **51**, 175–184.